This is a repository copy of *Solubility in Different Solvents, Crystal Polymorph and Morphology, and Optimization of Crystallization Process of AIBN*.

White Rose Research Online URL for this paper:
http://eprints.whiterose.ac.uk/127032/

Version: Accepted Version

Solubility of AIBN in Different Solvents, Crystal Polymorph and Morphology, and Optimization of Crystallization Process

Ya Jun Li[1], Kui Wu[1], Yang Li[1], Yang Zhang[1], Jing Jing Liu[2], and Xue Zhong Wang[1,2*]

[1]School of Chemistry and Chemical Engineering, South China University of Technology, Guangzhou, China 510640
[2]School of Chemical and Process Engineering, University of Leeds, Leeds LS2 9JT, UK

Correspondence authors:

Professor Xue Z. Wang
China One Thousand Talent Programme Professor
School of Chemistry and Chemical Engineering
South China University of Technology
381 Wushan Rd, Tianhe District
Guangzhou, PR China 510641
Tel.: +86 20 8711 4000, Fax: +86 20 8711 4000
Email: xuezhongwang@scut.edu.cn; Email: x.z.wang@leeds.ac.uk

Abstract

The solubility of 2, 2′-azobisisobutyronitrile (AIBN) in pure methanol, ethanol, acetone, benzene, ethyl acetate and a mixture of methanol and water was measured in the temperature range from 268.15 K to 325.15 K at atmospheric pressure. The AIBN solubility was sensitive to the temperature in all the pure solvents. The solubility in the binary mixture of methanol and water increased as the methanol fraction and temperature increased. The data were correlated with the modified Apelblat equation, Van't Hoff equation and Buchowski-Ksiazczak λh equation. Other results showed two AIBN polymorphs formed after the crystallization, form I, in a monoclinic cell, and form II, in a triclinic cell, which confirmed the two AIBN crystal structures reported in the literature. Additionally, the initial concentration and cooling rate of the AIBN crystallization had dominant roles in affecting the polymorphic forms of the AIBN crystals. The crystallization conditions were optimized in a 2 L crystallizer to yield crystals with the desired morphology and polymorphs, which resolved the caking issue experienced in the industrial production of AIBN. The optimized conditions were tested in a 20 L crystallizer.

Keywords: 2, 2′-azobisisobutyronitrile; solubility; polymorph; morphology; caking

1. Introduction

AIBN ($C_8H_{12}N_4$, CAS No. 78-67-1, IUPAC name: 2, 2′-azobisisobutyronitrile), which is shown in Figure 1, is a self-reactive material widely used as a blowing agent and initiator. Increasing interest has been shown regarding the synthesis and thermal decomposition characteristics of AIBN, which could result in thermal runaway due to its self-heating during storage or transportation[1-3]. In contrast, less attention has been paid to its purification via crystallization processes. Thus, the main aim of the present investigation was to study the crystallization of AIBN by focusing on the solubility of AIBN crystals in different solvents and the polymorphic forms and morphologies of the AIBN crystals. The second purpose of the study was to address a major challenge faced by AIBN crystalline solids, which is crystal caking.

The solubility of AIBN in pure solvents (methanol, ethanol, acetone, benzene and ethyl acetate) and a mixture of methanol and water was measured using a gravimetric method in the temperature range from 268.15 K to 325.15 K at atmospheric pressure. The data were correlated using the modified Apelblat equation, Van't Hoff equation and Buchowski-Ksiazczak λh equation. The solubility data and models were subsequently used in the design and optimization of the crystallization process. Under the optimized conditions, the crystals showed improved flowability, and the caking issue was resolved. The crystallization conditions were initially obtained in a 2 L crystallizer, and then, validated in a 20 L crystallizer.
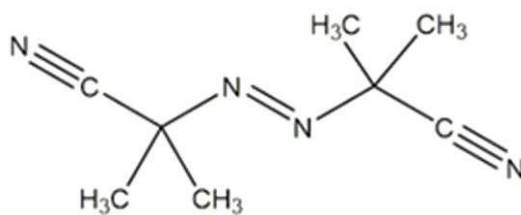
Figure 1. Molecular structure of AIBN.

2. Materials and Experiments

2.1 Materials

The AIBN used in this study was supplied by Shandong Haiming Chemical Industry Co., Ltd., China. After recrystallization, the obtained mass fraction purity was greater than 0.995, as analyzed by HPLC (Lc-20A, Shimadzu, Japan). The X-ray powder diffraction (XRPD) patterns of AIBN were obtained using an X-ray powder diffractometer (Bruker, Germany) at 40 KV, 40 mA, and a step size of 0.013° over the range 5° - 60°.

The XRPD pattern of the AIBN raw material is shown in Figure 2. The raw material was identified as form I (monoclinic) with characteristic diffraction peaks at 13.6, 16.2, 19.3, 26.9 and 30.6°[4]. The mass fraction purity values of the utilized materials are listed in Table 1.
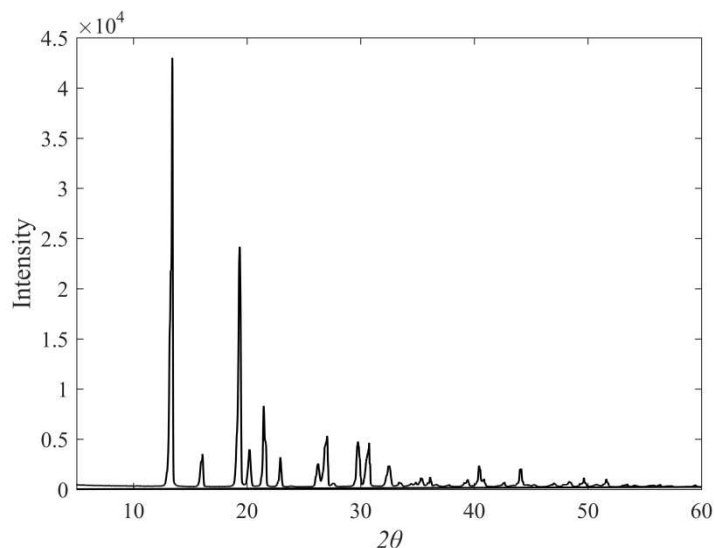
Figure 2. XRPD pattern of the AIBN raw material.

Table 1. Properties and Sources of Materials Used

chemical name	CAS registry number	source	purification method	mass fraction purity	analysis method
2,2′-azobisisobutyronitrile	78-67-1	Shandong Haiming Chemical Industry Co., Ltd.	Recrystallization from methanol	≥0.995	HPLC[a]
3-cyanopyridine	100-54-9	Guangzhou Lonza Co., Ltd.	none	≥0.990	HPLC[a]
methanol	67-56-1	Guangzhou Chemical Reagent Factory	none	≥0.995	GC[b]
ethanol	64-17-5	Nanjing Chemistry Reagent Co., Ltd.	none	≥0.997	GC[b]
acetone	67-64-1	Guangzhou Chemical Reagent Factory	none	≥0.995	GC[b]
benzene	71-43-2	Tianjin Fuyu Fine Chemical Industry Co., Ltd.	none	≥0.995	GC[b]
ethyl acetate	141-78-6	Sinopharm Chemical Reagent Co., Ltd.	none	≥0.995	GC[b]
deionized water	7732-18-5	Shanghai Xunhui Environment Technology Co., Ltd.	none	none	none

[a] High performance liquid chromatography. [b] Gas chromatography. The analysis method and the mass fraction purity of solvents were provided by the suppliers.

2.2 Apparatus and Procedure

The solubility measurements were conducted using a gravimetric method. A 150 mL jacketed glass reactor was used as the equilibrium cell. The jacketed glass reactor was constantly stirred by a magnetic stirrer (78-1, Changzhou Aohua Instrument Co., Ltd., China) to ensure that the AIBN solution remained uniform. The polymorphic forms of the AIBN crystals were obtained in a 50 mL double-jacketed glass crystallizer. The crystallization optimization experiments were carried out in a 2 L double-jacketed stirred glass crystallizer (DN 150, SCHOTT, Germany). The temperature was controlled by a circulating JULABO thermostatic water bath (FP51, JULABO, Germany) in all experiments. The temperature accuracy of the JULABO thermostatic was within 0.01 K. A Mettler Toledo AL204 electronic balance with an uncertainty of 0.1 mg was used to weigh all the samples. The DSC curves were measured using a differential scanning calorimeter (DSC 214, NETZSCH, Germany) in a nitrogen atmosphere with a heating rate of 10 K/min. Calibration of temperature and heat flow of the instrument were performed with indium before measurement. The digital images of the crystals were captured using a CCD color vision camera (MicroPublisher 3.3 RTV, QImaging, Canada) mounted on an Olympus BX53 optical microscope. The bulk density of the crystal products was measured using a powder characteristics tester (BT 100, Bettersizer Instrument Co., Ltd., China). A turbidity meter (PharmaVision (Qingdao) Intelligent Technology Ltd., China) was employed to determine the seeding temperature in the optimization of the crystallization process.

For solubility measurements below 313.15 K, we tested 12 h, 18 h and 24 h and determined that the system reached equilibrium in 12 h. For example, for equilibrium times of 12 h, 18 h and 24 h, the AIBN solubility ($m_{solute}/m_{solvent}$) in methanol at 298.15 K was 8.4558 g/100 g, 8.4343 g/100 g and 8.4660 g/100 g, respectively, which indicated that the system reached equilibrium in 12 h. For temperatures below 313.15 K, we assumed that 12 h was a sufficient time for the system to reach equilibrium.

However, for the experiments above 313.15 K, floccules formed in the solution if the same equilibrium time was used. This might be due to the decomposition of AIBN at high temperatures. As a result, we tested 6 h, 7 h and 8 h as the equilibrium times. For example, the solubility ($m_{solute}/m_{solvent}$) in methanol at 318.15 K was 25.7987 g/100 g, 25.7843 g/100 g and 25.8236 g/100 g, respectively. The solubility was very close, which indicated that the system reached equilibrium in 6 h. To reduce the risk of AIBN decomposition, 6 h was adopted as the equilibrium time for experiments that operated above 313.15 K.

First, approximately 100 mL of solvent was placed into a jacketed glass reactor. The reactor was maintained at a set temperature. Next, excess AIBN was added into the reactor at a constant temperature. The slurry was stirred for 12 h if the temperature was below 313.15 K or 6 h if the temperature was above 313.15 K. After 12 h or 6 h, the stirring was stopped, and the system was maintained at that temperature for another 12 h or 6 h. Afterwards, approximately 5 mL of the clear upper solution was withdrawn and placed into a weighing bottle (weight m_0) using a preheated syringe. The temperature was measured using a calibrated thermometer with an uncertainty of 0.05 K and simultaneously recorded. The bottle containing the sample solution was quickly weighed (m_1) and dried in a fume hood for 5 h at room temperature. The residual solids were obtained after filtration. Finally, the products were transferred to a vacuum oven. The temperature of the vacuum oven was 298.15 K. The weighing bottle was weighed (m_2) after drying in the vacuum oven for 24 h. After 24 h, the sample was considered fully dried because the weight of the sample was constant even after a longer time in the oven. We also tested 48 h. The XRPD patterns of the residual solids and dried crystals from the supernatant were characterized.

The mole fraction of AIBN (x_A) in the pure solvents and mixture of methanol and water was calculated using eq. 1, and the mass fraction of the binary solvent, wt, was defined by eq. 2.

$$x_A = \frac{m_A/M_A}{m_A/M_A + m_B/M_B + m_C/M_C} \tag{1}$$

$$wt = \frac{m_B}{m_B + m_C} \tag{2}$$

In the mixture of methanol and water, m_A, m_B and m_C represent the masses of AIBN, methanol and water, respectively. M_A, M_B and M_C are the molecular weights of AIBN, methanol and water, respectively. In pure solvents, m_A and m_B are the masses of the solute and solvent, respectively. M_A and M_B represent the molecular weights of the solute and solvent, respectively, and m_c=0. Each solubility data point was the average of three parallel measurements.

To verify the reliability and accuracy of the experimental method, a set of verification measurements were conducted in which the mole fraction solubility of 3-cyanopyridine (3-CNP) in acetone was measured. The experimental measured solubility was compared with data from literature[5], as presented in Table 2. The relative deviation (RD) between the literature and experimental data is less than 2.62%. It showed good consistency, indicating the reliability of experimental methods and apparatus used in this study.

Table 2. Comparison of Experimental Solubility of 3-CNP in acetone at (273.15 to 318.15) K (0.1 Mpa)

	a with Data Reported in the Literature		
T/K	$(10^4 x_A^{lit})^b$	$(10^4 x_A^{exp})^c$	100RD
273.15	29.0	29.73	2.46
278.15	32.9	33.41	1.53
288.15	43.8	43.66	-0.32
298.15	54.1	52.98	-2.11
308.15	66.4	67.17	1.15
318.15	83.3	85.54	2.62

a The standard uncertainties u are u(T)=0.05 K and u(P)=5 KPa. The relative standard uncertainty of the solubility measurement is u_r (x_A)=0.02. RD refers to the relative deviation between the experimental and reported solubility. b x_A^{lit} is mole fraction solubility of 3-CNP in acetone at temperature T reported in the literature[5]. c x_A^{exp} is mole fraction solubility of 3-CNP in acetone at temperature T determined in this work.

3. Thermodynamic Models

The AIBN solubility in pure solvents and a mixture of methanol and water were correlated using the thermodynamic models described below.

3.1 Modified Apelblat Equation

Eq. 3 represents the modified Apelblat equation, which is a semi-empirical model with the following expression[6-8]:

$$\ln(10^4 x_A) = A + B/T + C\ln(T)$$

(3)

where x_A is the mole fraction solubility, T is the absolute temperature, and A, B and C are empirical constants.

3.2 *Van't Hoff Equation*

The Van't Hoff model is also widely used to model the relationships between the mole fraction solubility, temperature, enthalpy of dissolution and entropy of dissolution[9-10]:

$$\ln(10^4 x_A) = -\Delta H/RT + \Delta S/R$$

(4)

where x_A is the mole fraction solubility, T is the absolute temperature, R is the gas constant, and ΔH and ΔS represent the enthalpy of dissolution and entropy of dissolution, respectively. ΔH and ΔS are assumed to be independent of the temperature within a certain temperature range.

3.3 Buchowski-Ksiazczak *λh* Equation

The Buchowski-Ksiazczak *λh* equation is another model that can be used to correlate solid-liquid equilibria[11-12].

$$\ln\left[1+\lambda\frac{1-x_A}{x_A}\right]=\lambda h(\frac{1}{T}-\frac{1}{T_m})$$

(5)

where x_A is the mole fraction solubility, T is the absolute temperature, T_m is melting point, λ and h are the model parameters.

3.4 Model Building

A partial least-squares (PLS) approach was used to calibrate the parameters of the three models using the solubility data.

The relative deviation (RD) between the experimental data and the predictions was calculated using eq. 6.

$$RD=\left(x_A-x_{A,calc}\right)\big/x_A$$

(6)

The relative average deviation (RAD) was employed to assess the accuracy of the developed models:

$$RAD=\frac{1}{N}\sum_{i}^{n}\left|\frac{x_A-x_{A,calc}}{x_A}\right|$$

(7)

where N is the number of experimental points, and x_A and $x_{A,calc}$ represent the experimental and calculated values of the solubility, respectively.

4 Results and Discussion

4.1 Solubility in Pure Solvents
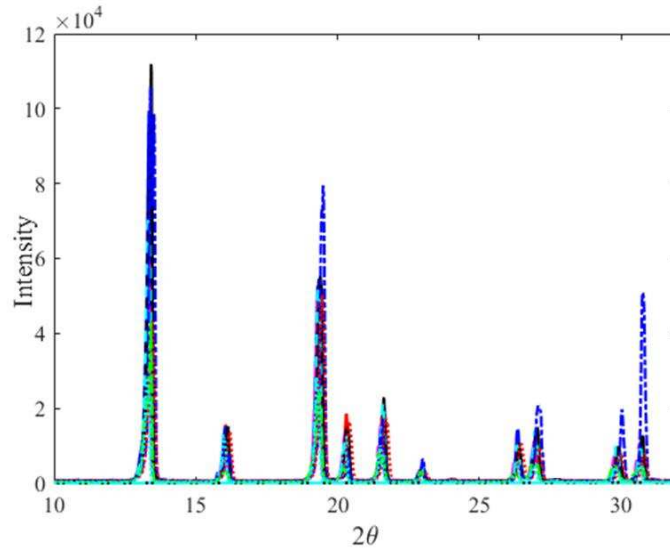
Figure 3. Ten XRPD patterns of AIBN residual solids and crystals from the supernatant obtained in the solubility experiments, methanol at 313.15 K (―― residual solids and --- crystals from the supernatant), ethanol at 317.65 K (―― residual solids and --- crystals from the supernatant), acetone at 302.95 K (―― residual solids and --- crystals from the supernatant), benzene at 312.65 K (— - —residual solids and ···crystals from the supernatant), ethyl acetate at 298.35 K (— - —residuals solids and ··· crystals from

the supernatant), showing that the solids remained in form I.
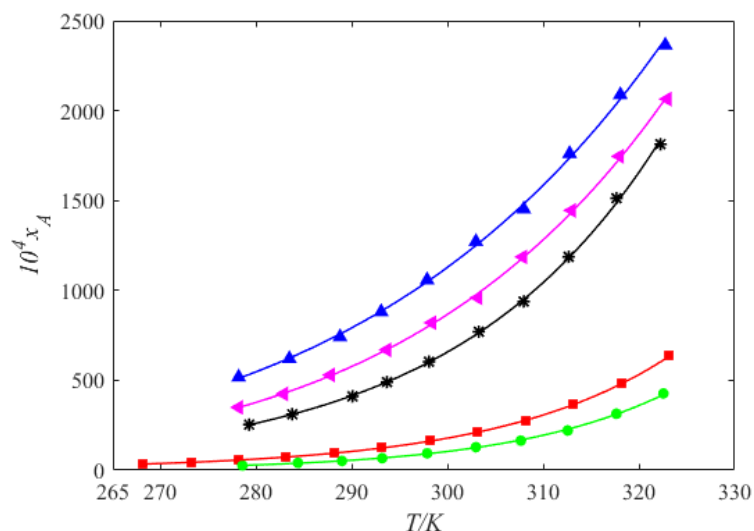
Figure 4. The solubility of AIBN in pure solvents: ■, methanol; ●, ethanol; ▲, acetone; ※, benzene; ◄, ethyl acetate. The solid curves are the correlations from the modified Apelblat model.

The XRPD patterns of the residual solids and dried crystals from the supernatant for all the solubility experiments were characterized, and some of the results are shown in Figure 3. Form I (monoclinic) crystals were identified, which were the same as the raw materials. This showed that the measured data were for the solubility of AIBN crystals in form I. The AIBN mole fraction solubility in pure methanol, ethanol, acetone, benzene and ethyl acetate at different temperatures is summarized in Table 3 and Figure 4. Table 3 also shows the fitted solubility for the pure solvents using the proposed models, and the fitting parameters are given in Table 4.

Table 3. Experimental and Model-fitted (eq. 3-5) AIBN Solubility in Methanol, Ethanol, Acetone, Benzene and Ethyl Acetate (0.1 Mpa)[a]

T/K	$10^4 x_A$	eq. 3	100RD	eq. 4	100RD	eq. 5	100RD
Methanol							
268.15	34.00	34.20	-0.60	30.69	9.72	33.52	1.39
273.15	44.08	43.89	0.44	42.03	4.67	44.35	-0.60
278.15	56.69	56.57	0.20	56.90	-0.37	58.13	-2.55
283.15	73.84	73.20	0.86	76.21	-3.21	75.56	-2.34
288.15	94.21	95.05	-0.89	101.05	-7.26	97.46	-3.45
293.15	123.65	123.81	-0.13	132.70	-7.32	124.82	-0.95
298.15	162.31	161.70	0.38	172.68	-6.39	158.86	2.13
303.15	212.00	211.70	0.14	222.75	-5.07	201.06	5.16
308.15	276.64	277.74	-0.40	284.99	-3.02	253.25	8.45
313.15	364.02	365.04	-0.28	361.76	0.62	317.74	12.71
318.15	479.26	480.56	-0.27	455.79	4.90	397.44	17.07
323.15	636.89	633.47	0.54	570.15	10.48	496.12	22.10
Ethanol							

9

278.55	26.25	26.88	-2.41	25.51	2.81	26.41	-0.62
284.35	40.81	38.92	4.62	38.51	5.64	39.17	4.02
288.95	51.14	52.12	-1.92	52.75	-3.16	52.97	-3.58
293.15	66.66	67.96	-1.95	69.72	-4.58	69.25	-3.88
297.85	93.78	91.34	2.61	94.36	-0.61	92.71	1.14
302.95	128.30	125.66	2.05	129.66	-1.06	126.10	1.71
307.65	164.51	168.32	-2.32	172.17	-4.65	166.18	-1.01
312.55	220.99	227.89	-3.13	229.30	-3.76	220.04	0.43
317.65	314.01	311.78	0.71	306.08	2.52	292.77	6.77
322.55	426.54	420.53	1.41	400.52	6.10	383.12	10.18

<div align="center">Acetone</div>

278.15	517.62	510.79	1.32	503.94	2.64	510.69	1.34
283.45	620.13	623.48	-0.54	621.33	-0.19	625.79	-0.91
288.75	740.96	757.56	-2.24	760.19	-2.60	761.44	-2.76
293.05	881.06	884.39	-0.38	890.57	-1.08	888.48	-0.84
297.85	1058.11	1047.76	0.98	1056.96	0.11	1050.37	0.73
302.95	1271.14	1249.94	1.67	1260.43	0.84	1248.17	1.81
307.95	1452.88	1480.76	-1.92	1489.43	-2.52	1470.88	-1.24
312.75	1760.61	1736.87	1.35	1739.57	1.20	1714.50	2.62
318.05	2087.91	2064.28	1.13	2053.62	1.64	2021.24	3.19
322.75	2364.22	2398.87	-1.47	2368.43	-0.18	2329.97	1.45

<div align="center">Benzene</div>

279.25	253.67	252.71	0.38	242.03	4.59	250.24	1.35
283.75	311.29	310.79	0.16	306.43	1.56	313.04	-0.56
290.05	410.80	415.49	-1.14	421.17	-2.53	423.35	-3.05
293.65	490.10	490.61	-0.10	502.03	-2.43	500.15	-2.05
298.05	603.25	601.21	0.34	618.64	-2.55	609.87	-1.10
303.25	770.12	764.57	0.72	785.69	-2.02	765.32	0.62
307.95	938.20	950.10	-1.27	968.42	-3.22	933.55	0.50
312.65	1186.82	1180.52	0.53	1186.17	0.06	1132.09	4.61
317.65	1513.00	1486.96	1.72	1462.14	3.36	1381.32	8.70
322.25	1813.10	1838.15	-1.38	1762.28	2.80	1649.97	9.00

<div align="center">Ethyl acetate</div>

278.15	349.26	348.48	0.22	343.15	1.75	347.00	0.65
282.85	424.07	427.06	-0.70	425.04	-0.23	428.01	-0.93
287.75	529.73	525.63	0.77	527.36	0.45	528.85	0.17
293.65	669.50	671.15	-0.25	677.24	-1.16	676.03	-0.98
298.35	820.71	811.98	1.06	820.76	-0.01	816.50	0.51
303.15	959.48	982.69	-2.42	992.63	-3.45	984.32	-2.59
307.85	1186.61	1180.43	0.52	1188.90	-0.19	1175.58	0.93
312.95	1444.77	1434.84	0.69	1437.17	0.53	1417.12	1.91
317.95	1746.08	1731.04	0.86	1720.65	1.46	1692.58	3.06
322.95	2064.36	2081.08	-0.81	2048.59	0.76	2011.08	2.58

[a]Eq. 3 pertains to the modified Apeblat equation. Eq. 4 refers to the Van't Hoff model. Eq. 5 represents the Buchowski-Ksiazczak λh equation. x_A is the experimental AIBN solubility data. RD refers to the relative deviation between the experimental and model fitted solubility. The standard uncertainties u are u(T)=0.05 K and u(P)=5

The experimental solubility of AIBN in methanol was compared with data from literature[13], as shown in Figure S1 in the supporting information of this article. It showed good consistency, and the minor deviations might be caused by instrumental and measurement errors. In particularly, the laser dynamic method was applied for the measurement of solubility in the literature, and a gravimetric method was used in this work. The different measurement methods could also contribute to the minor deviations.

Figure 4 indicated that the AIBN solubility in all the pure solvents within the temperature range increased as the temperature increased, and the magnitude of the increase with the temperature was different for each solvent in the following order: $x_{A,acetone} > x_{A,ethyl\ acetate} > x_{A,benzene} > x_{A,methanol} > x_{A,ethanol}$. This suggested that the polarity of the solvent was not the only factor that affected the AIBN solubility since the polarity values are in a different order: methanol (76.2) > ethanol (65.4) > acetone (35.5) > ethyl acetate (23) > benzene (11.1)[14]. Since both hydrophilic (cyano group, -CN) and hydrophobic groups (methyl group, -CH$_3$) exist in AIBN, the hydrogen bonding interactions between the solute and solvent also play a role in the solubility in different solvents.

The solubility data in different solvents provide fundamental data to optimize the crystallization conditions and yield. Table 5 lists the RAD results using the different correlation models. The average RAD values of the three proposed models were 1.13% (Apelblat), 2.71% (Van't Hoff) and 3.23% (λh). Therefore, the modified Apelblat model best fit the experimental solubility of AIBN in pure solvents.

Table 4. Parameters of the Apelblat, Van't Hoff and Buchowski-Ksiazczak λh Models Obtained in Pure Solvents

model	parameter	methanol	ethanol	acetone	benzene	ethyl acetate
Apelblat	A	-250.34	-185.07	-35.91	-167.24	-44.75
	B	7313.07	3697.94	-732.04	4234.86	-748.07
	C	40.52	31.10	7.96	27.98	9.47
Van't Hoff	ΔH	38275.32	46752.07	25898.95	34544.85	29787.41
λh	λ	0.26	0.40	0.86	0.98	0.95
	h	15418.52	13326.33	3499.79	4039.35	3700.27

Table 5. 100RAD for the Different Models in Pure Solvents

model	methanol	ethanol	acetone	benzene	ethyl acetate
Apelblat	0.43	2.31	1.30	0.77	0.83
Van't Hoff	5.25	3.49	1.30	2.51	1.00
λh	6.57	3.33	1.69	3.15	1.43

4.2 Solubility in Binary Solvent Mixtures
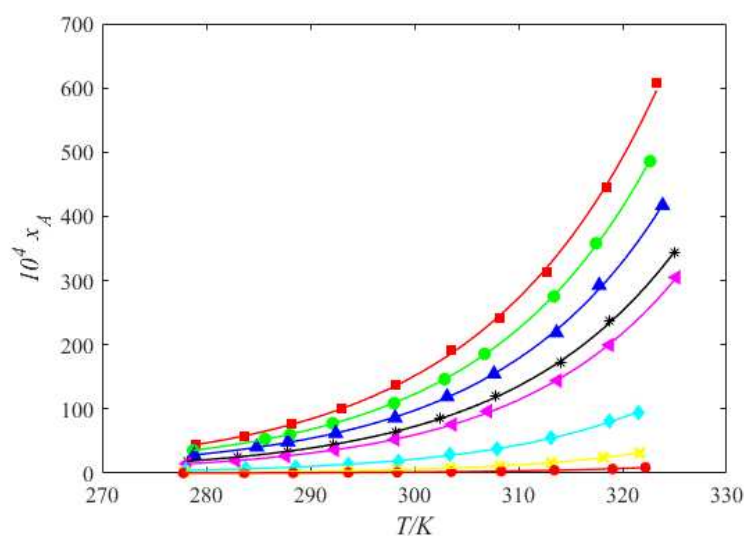
Figure 5. AIBN solubility in a mixture of methanol and water: ■, (wt=0.95); ●, (wt=0.90); ▲, (wt=0.85); ※, (wt=0.80); ◄, (wt=0.75); ◆, (wt=0.60); ×, (wt=0.45); ●, (wt=0.30). The solid lines represent the correlated values using the modified Apelblat model.

Methanol is used as a solvent for industrial cooling crystallization of AIBN, and water is brought into the crystallizers during the recycling of the solvent. The residual solids and dried AIBN crystals from the supernatant in methanol-water systems also crystallized in the monoclinic form. The AIBN mole fraction solubility in a mixture of methanol and water at different temperatures is summarized in Table 6 and Figure 5. Table 6 also illustrates the solubility fits for binary mixtures based on the three models, and the results are given in Table 7. The data indicated that the AIBN solubility in the mixture of methanol and water increased as the temperature and fraction of methanol increased.

Table 6. Experimental and Model-fitted (eq. 3-5) AIBN Solubility in a Mixture of Methanol (wt) and Water (1-wt) (0.1 Mpa)[a]

T/K	$10^4 x_A$	eq. 3	100RD	eq. 4	100RD	eq. 5	100RD
			wt=0.95				
279.05	44.38	44.51	-0.29	41.98	5.40	43.89	1.11
283.65	57.79	58.15	-0.62	57.10	1.19	58.55	-1.31
288.25	76.28	76.04	0.31	76.90	-0.81	77.43	-1.51
292.95	101.18	100.12	1.05	103.24	-2.03	102.19	-1.00
298.25	136.34	136.64	-0.23	142.31	-4.38	138.43	-1.53
303.55	191.53	186.61	2.57	193.99	-1.28	185.84	2.97
308.15	241.71	244.65	-1.22	251.65	-4.11	238.38	1.38
312.75	312.06	320.81	-2.80	323.95	-3.81	304.10	2.55
318.45	445.54	448.85	-0.74	438.54	1.57	408.47	8.32

12

323.25	606.87	595.50	1.87	561.27	7.51	521.20	14.12
			wt=0.90				
278.75	35.45	35.45	0.01	32.84	7.36	35.00	1.27
285.65	53.17	52.77	0.76	52.39	1.48	53.66	-0.92
288.05	59.93	60.69	-1.28	61.30	-2.30	61.99	-3.44
292.15	77.87	77.23	0.82	79.71	-2.37	78.92	-1.36
298.05	108.93	109.62	-0.63	114.84	-5.43	110.60	-1.53
302.90	146.46	146.59	-0.09	153.40	-4.74	144.77	1.16
306.75	185.89	184.92	0.53	191.77	-3.16	178.41	4.02
313.40	275.32	276.96	-0.60	278.41	-1.12	253.79	7.82
317.45	358.00	354.75	0.91	346.70	3.16	313.11	12.54
322.65	485.96	488.15	-0.45	455.79	6.21	408.38	15.96
			wt=0.85				
278.85	28.12	28.53	-1.47	26.36	6.23	27.97	0.53
284.85	40.71	40.17	1.33	39.61	2.71	40.69	0.05
287.85	48.74	47.77	1.98	48.24	1.02	48.82	-0.17
292.45	62.02	62.50	-0.77	64.76	-4.41	64.13	-3.41
298.15	86.14	87.55	-1.64	92.10	-6.93	89.03	-3.36
303.15	119.06	118.06	0.83	124.08	-4.22	117.74	1.10
307.65	154.70	154.89	-0.12	160.93	-4.02	150.53	2.69
313.65	218.77	223.13	-1.99	224.98	-2.84	207.33	5.23
317.75	292.54	286.84	1.95	280.81	4.01	256.98	12.16
323.85	416.95	417.78	-0.20	386.49	7.31	352.03	15.57
			wt=0.80				
278.15	18.82	18.69	0.74	17.49	7.11	18.56	1.43
282.95	24.94	25.17	-0.93	24.64	1.19	25.44	-2.01
287.75	33.93	33.92	0.01	34.32	-1.17	34.53	-1.79
292.25	44.77	44.90	-0.27	46.37	-3.56	45.61	-1.88
298.15	64.52	64.86	-0.52	67.85	-5.16	64.98	-0.72
302.45	85.86	84.81	1.22	88.71	-3.32	83.50	2.74
307.85	119.43	118.78	0.55	122.91	-2.91	113.54	4.93
314.05	172.15	174.79	-1.54	176.26	-2.39	160.14	6.98
318.75	236.58	234.19	1.01	229.51	2.99	206.74	12.61
324.95	343.20	344.23	-0.30	321.34	6.37	288.11	16.05
			wt=0.75				
278.15	14.69	14.54	0.99	13.56	7.64	14.46	1.55
282.85	19.48	19.67	-1.02	19.23	1.27	19.91	-2.21
287.65	26.74	26.82	-0.31	27.14	-1.52	27.32	-2.18
292.35	36.30	36.35	-0.12	37.62	-3.63	36.90	-1.65
298.15	52.50	52.92	-0.81	55.50	-5.71	52.87	-0.72
303.65	75.75	75.60	0.20	79.14	-4.48	73.58	2.86
307.05	96.56	94.25	2.39	97.93	-1.42	89.84	6.96
313.75	144.29	145.51	-0.85	147.02	-1.89	131.97	8.54
318.75	199.64	201.16	-0.76	196.90	1.37	174.70	12.49
325.15	305.02	304.29	0.24	282.43	7.41	248.69	18.47

	wt=0.60						
278.05	4.38	4.44	-1.40	4.25	2.94	4.39	-0.22
283.75	6.93	6.78	2.18	6.72	3.06	6.82	1.55
288.55	9.55	9.63	-0.84	9.74	-1.97	9.76	-2.23
293.65	14.38	13.92	3.18	14.26	0.82	14.12	1.80
298.45	18.77	19.61	-4.45	20.18	-7.49	19.78	-5.34
303.45	28.37	27.89	1.71	28.63	-0.92	27.81	1.98
307.90	37.10	38.02	-2.46	38.72	-4.37	37.38	-0.75
313.15	55.38	54.55	1.50	54.68	1.26	52.55	5.10
318.70	80.75	79.49	1.56	77.79	3.67	74.71	7.49
321.55	95.08	96.26	-1.24	92.78	2.42	89.26	6.13
	wt=0.45						
277.90	1.14	1.12	1.11	1.03	9.00	1.12	1.25
283.65	1.73	1.73	-0.10	1.71	1.55	1.77	-1.98
288.45	2.41	2.49	-3.32	2.55	-5.58	2.54	-5.41
293.65	3.79	3.71	2.18	3.88	-2.46	3.73	1.49
298.35	5.22	5.31	-1.75	5.61	-7.48	5.22	-0.11
303.45	8.07	7.85	2.79	8.25	-2.18	7.44	7.81
308.20	11.16	11.30	-1.27	11.68	-4.68	10.26	8.05
313.15	16.67	16.54	0.80	16.60	0.43	14.23	14.66
318.15	24.36	24.30	0.25	23.41	3.90	19.66	19.30
321.65	31.56	31.82	-0.85	29.60	6.21	24.58	22.12
	wt=0.30						
277.80	0.31	0.30	1.59	0.28	9.35	0.30	1.76
283.65	0.46	0.47	-3.34	0.46	-1.65	0.48	-5.12
288.35	0.67	0.67	-0.08	0.69	-2.11	0.69	-1.90
293.65	1.04	1.01	3.46	1.05	-0.99	1.01	2.96
298.35	1.39	1.44	-2.98	1.51	-8.67	1.41	-1.21
303.55	2.18	2.13	2.47	2.24	-2.50	2.02	7.53
308.35	2.99	3.07	-2.69	3.17	-6.23	2.79	6.65
313.45	4.70	4.52	3.85	4.54	3.34	3.90	17.09
319.05	6.57	6.92	-5.28	6.65	-1.23	5.58	14.99
322.20	9.01	8.79	2.52	8.19	9.11	6.82	24.35

[a]Eq. 3 pertains to the modified Apelblat equation. Eq. 4 refers to the Van't Hoff model. Eq. 5 represents the Buchowski-Ksiazczak λh equation. x_A is the experimental AIBN solubility data. Wt is the initial mass fraction of methanol in the binary solvent mixtures. RD refers to the relative deviation between the experimental and model-fitted solubility. The standard uncertainties u are u(T)=0.05 K and u(P)=5 KPa. The relative standard uncertainty of the solvent composition is u_r(Wt)=0.01. The relative standard uncertainty of the solubility measurement is u_r(x_A)=0.05.

Table 7. Parameters of the Apelblat, Van't Hoff and Buchowski-Ksiazczak λh
Models for AIBN in a Mixture of Methanol and Water

model	parameter	wt=0.95	wt=0.90	wt=0.85	wt=0.80	wt=0.75	wt=0.60	wt=0.45	wt=0.30
Apelblat	A	-225.78	-277.83	-289.60	-228.99	-241.65	-150.94	-308.18	-293.86

	B	5827.17	8063.18	8591.26	5662.50	6032.60	1484.62	8005.51	7361.22
	C	37.06	44.84	46.56	37.59	39.56	26.14	49.67	47.30
Van't Hoff	ΔH	43997.88	44805.33	44802.13	46745.27	48575.00	52696.68	56974.78	56562.98
λh	λ	0.43	0.34	0.28	0.24	0.22	0.14	0.04	0.01
	h	11422.72	14443.70	17802.20	21837.36	24362.93	44103.02	156755.05	594271.43

Using the model parameters from eq. 4, the enthalpy of AIBN dissolution was calculated, and the data are shown in Table 7. The enthalpy of AIBN dissolution in all the solvents was positive, which indicated the dissolution of AIBN in all the solvents was endothermic. Therefore, the growth of crystals from the solutions should be exothermic[10]. Table 8 lists the RAD values obtained with the different correlation models. The average RAD values were 1.35% (Apelblat), 3.79% (Van't Hoff) and 5.47% (λh). Therefore, the modified Apelblat model best fit the experimental AIBN solubility in the binary mixture.

Table 8. 100RAD of the Different Models in a Mixture of Methanol and Water

model	wt=0.95	wt=0.90	wt=0.85	wt=0.80	wt=0.75	wt=0.60	wt=0.45	wt=0.30
Apelblat	1.17	0.61	1.23	0.71	0.77	2.05	1.44	2.83
Van't Hoff	3.21	3.73	4.37	3.62	3.63	2.89	4.35	4.52
λh	3.58	5.00	4.43	5.11	5.76	3.26	8.22	8.36

4.3 Polymorphic Forms of the AIBN Crystals

Jaffe et al.[15] reported two AIBN crystal cell structures, a monoclinic cell (lattice parameters of a=5.509 (1,2), b=8.225 (2,1), c=11.002 (2,1) Å, and β=96.00 (1,1)°) and a triclinic cell (cell parameters of a=7.865(2), b=5.555(1), c=6.201(1) Å, α=71.33(1)°, β=77.95(2)°, and γ=79.19(2)°). However, little is known regarding the preparation of the two AIBN polymorphs via crystallization. Here, experiments were designed to investigate the polymorph conversion based on the measured solubility data.

The experiments were performed in a 50 mL double-jacketed glass crystallizer, and the temperature was controlled using a JULABO refrigerated and heating circulator. The jacketed glass crystallizer was constantly stirred, and the experimental design is shown in Table 9.

Table 9. Operation Conditions for the Polymorph Conversion Study

run	AIBN mass (g)	initial temperature (K)	final temperature (K)	cooling rate (K/min)	polymorph
P1	4.20	313.15	278.15	1	I
P2	4.20	313.15	278.15	0.5	I
P3	4.20	313.15	278.15	0.25	II
P4	3.53	313.15	278.15	1	II
P5	3.53	313.15	278.15	0.5	I
P6	3.53	313.15	278.15	0.25	I

Slurry samples were prepared by adding a certain amount of AIBN into 25 g of methanol (Table 9). The

mixture was then quickly heated to 313.15 K and held at that temperature for 20 min. The AIBN completely dissolved under constant stirring, and the solution was then cooled to 278.15 K at a given cooling rate. After reaching the set temperature, the slurry was stirred for another 1 h. The resulting products were filtered off and dried under a fume hood for 10 h, and the solid phase composition was quantified by XRPD.
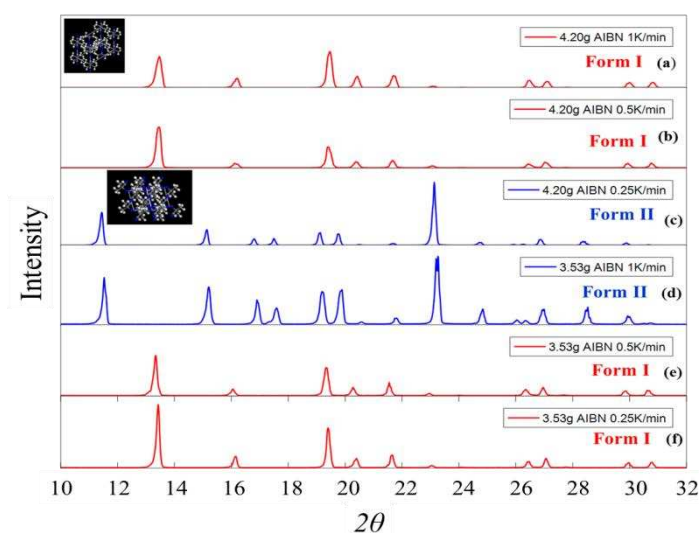
Figure 6. The XRPD patterns of the AIBN crystals prepared via the addition of different AIBN amounts and different cooling rates: (a) form I: 4.20 g at 1 K/min; (b) form I: 4.20 g at 0.5 K/min; (c) form II: 4.20 g at 0.25 K/min; (d) form II: 3.53 g at 1 K/min; (e) form I: 3.53 g at 0.5 K/min; (f) form I: 3.53 g at 0.25 K/min.

The AIBN raw material is form I (monoclinic), as illustrated in Figure 2. The XRPD patterns of the crystalline products obtained under the conditions listed in Table 9 are shown in Figure 6. The data indicated that the conditions of experiment P1 resulted in a product polymorph that was the same as that of the raw materials (Figure 6(a)). Additionally, the polymorph conversion of AIBN was not observed with a higher initial concentration and fast cooling rate, but the crystals prepared at a lower initial concentration and the same cooling rate (experiment P4) had different patterns (Figure 6(d)). The characteristic diffraction peaks of P4 were recorded at 11.9, 15.3, 17.5, 19.7, 23.1, 25.0, 27.0, 28.7 and 30.4°, which were consistent with those of the triclinic crystals[4]. Another form (form II) crystallized in a triclinic cell, which demonstrated that the initial concentration played an important role in the polymorph conversion of AIBN.
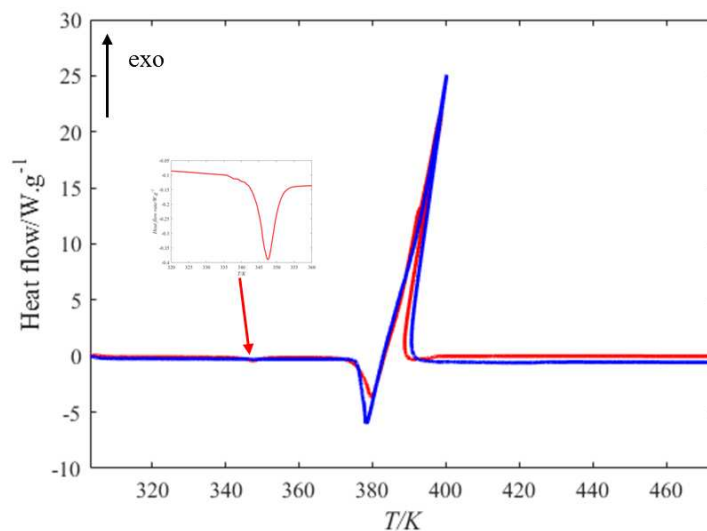
Figure 7. The DSC curves of the two AIBN forms. The red line shows form I (monoclinic), and the blue line shows form II (triclinic).

The DSC data for the two polymorphic forms of AIBN were measured from 303.15 to 473.15 K at a heating rate of 10 K/min, and the results are shown in Figure 7. An endothermic peak appeared at 373.15-383.15 K for both forms, which was related to the AIBN melting. The decomposition was a single exothermic peak and occurred at approximately 383.15 K in the liquefied state for both forms. However, a small endothermic peak was observed in the DSC traces of form I, which was due to the phase transition. The phase transition point (T_p) of AIBN form I was found to be 343.86 K, and the uncertainty u was u(T_p)=0.3 K. In other words, the AIBN that crystallized in the monoclinic (form I) form transformed into the more stable triclinic form (form II)[1, 4, 16]. The solid-solid transformation did not significantly influence the much larger exothermic peak related to the AIBN decomposition.

A comparison of the experimental results of P1, P2 and P3 (Figure 6(a, b, c)) clearly showed that for a higher initial concentration, the polymorph of the crystals changed from form I to form II as the cooling rate slowed down from 0.5 K/min to 0.25 K/min. At a low initial concentration (Figure 6 (d, e, f)), the product's polymorph changed to form II after the cooling rate increased from 0.5 K/min to 1 K/min. The polymorphic phase transition in the crystallization often occurs via three mechanisms: (1) primary nucleation of the more stable solid phase. Once the nucleation begins, the growth of the stable phase induces a decrease in the concentration until the solubility of the metastable phase is reached; (2) dissolution of the metastable solid phase; and (3) growth of the more stable solid via mass transfer of the solute in solution[17-18]. The three mechanisms are either consecutive or concomitant. Thus, the variables that

17

influence the phase transition include supersaturation, the temperature, the medium, the hydrodynamics, and the crystal habit and particle size. In this work, the initial concentration and cooling rate both influenced the supersaturation and, therefore, the phase transition.

4.4 Tailoring the Morphology of the AIBN Crystals

A major challenge in producing AIBN crystal solids is caking, which greatly affects the transportation, storage and use of the product. Crystal caking can occur due to the absorption and desorption of the moisture content and often has three stages, moisture sorption, liquid bridge effects and crystal bridge formation[19,20]. The manufacturer of the AIBN crystalline product has improved their drying process, but the caking problem still exists. The literature has also reported that the caking issue can be addressed by improving the crystal shape[21]. A round crystal shape often results in better flowability and improved caking performance.

The crystal morphology is considered a possible cause of AIBN caking. Industrial AIBN-based products are long rod-like crystals with a small bulk density and poor flowability. However, sphere-like or cubic-like crystals usually have larger bulk densities and better flowability, and they can prevent caking. We attempted to address this issue by optimizing the crystallization process to obtain a product with an ideal morphology, which can prevent the AIBN from caking. The optimized operation conditions were first investigated in a lab-scale crystallizer and validated in a pilot-scale production.

The cooling rate was found to have a major impact on the morphology of the AIBN crystals in the early stages of the AIBN crystallization. The effect of the cooling rate and the agitation speed on the crystal performances was first investigated in a 2 L double-jacketed stirred glass crystallizer. A slurry sample was prepared by adding 300 g of AIBN to 900 g of methanol in the crystallizer. The mixture was then quickly heated to 323.15 K under constant stirring and held at that temperature until a complete dissolution was achieved. Next, the solution was cooled to 278.15 K with different cooling rates and stirring speeds (Table 10).

Table 10. The Operation Conditions for the Morphology Optimization Experiments

run	mass of AIBN (g)	cooling rate (K/min)	agitation speed (rpm)
M1	300	0.5	400
M2	300	0.5	150
M3	300	0.25	400
M4	300	0.25	250
M5	300	0.25	150
M6	300	0.1	400
M7	300	0.1	150
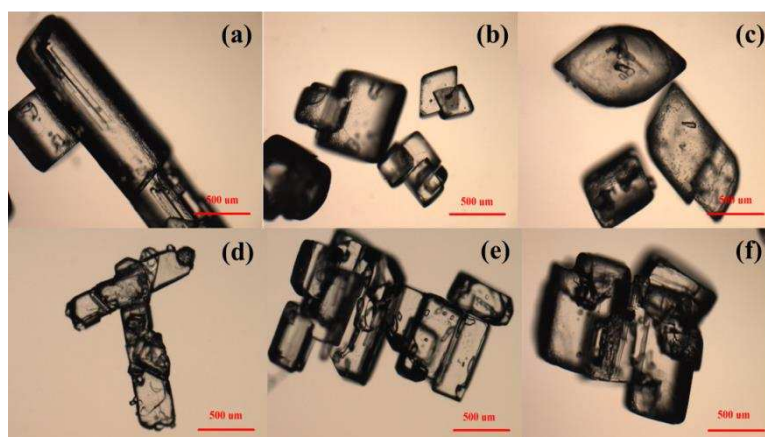
Figure 8. The crystal morphologies from the experiments in Table 10: (a) M1: 400 rpm, 0.5 K/min; (b) M2: 400 rpm, 0.25 K/min; (c) M3: 400 rpm, 0.1 K/min; (d) M5: 150 rpm, 0.5 K/min; (e) M6: 150 rpm, 0.25 K/min; (f) M7: 150 rpm, 0.1 K/min.
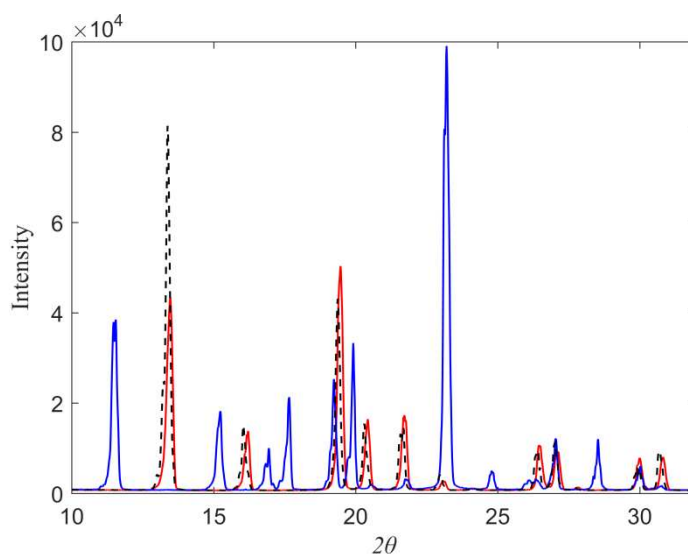
Figure 9. The XRPD patterns of the AIBN products. The black line represents experiment M6, the red line shows form I, and the blue line depicts form II.
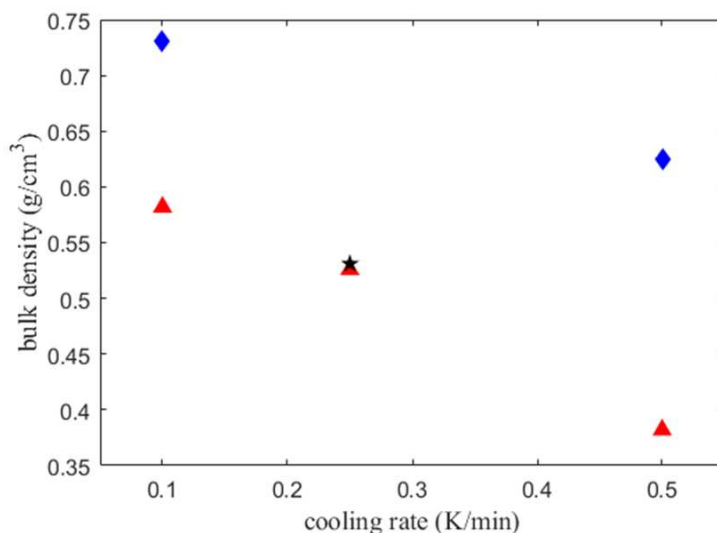
Figure 10. The bulk density of the crystalline products: ▲: 150 rpm; ★: 250 rpm; ◆: 400 rpm.

Figure 8 shows the microscopic images of the crystals obtained under different operational conditions. As the cooling rate decreased from 0.5 K/min to 0.1 K/min, the AIBN morphology changed from rod-like to cubic-like. At a higher agitation speed of 400 rpm, the crystal shapes appeared to be more spherical, and despite the obvious changes in the crystal morphology, the polymorph of the products was form I, which was similar to that of the raw materials in experiment M6 (Figure 9).

The bulk density of the crystal products was measured using a Powder Integrative Characteristics Tester, and the data are shown in Figure 10. Decreasing the cooling rate and increasing the agitation speed both improved the bulk density, and higher values were obtained for the crystals produced by experiment M6. Compared to that of the rod-like crystals, both the cubic-like and sphere-like crystals have reduced contact areas among the crystals, which increased the bulk density, improved the flowability and prevented caking.

In addition to the flowability, the crystallization process must meet multiple objectives, including higher yields and reduced production time. Although the optimized conditions (M6) produced sphere-like crystals and significantly improved the bulk density, the operation time was 450 minutes, which is considered long. Seeding is an effective approach to optimize a batch crystallization process and obtain crystal products with the desired size distribution or morphology. This could consume the supersaturation generated by the cooling and restrain the secondary nucleation by growing seeds. Consequently, the addition of crystal seeds and an increase in the cooling rate were used to decrease the operation time. The size, morphology, amount of seeds added and seeding temperature should all be determined before the optimization.

Based on the morphology optimization (Figure 8), the recrystallized crystals from M6 with sphere-like

shapes were used as the seeds after sieving. Meanwhile, the rod-like crystals from M1 were also used as seeds to examine the impact of the seed morphology on the final product morphology. The desired size of the seeds ranged between 200 and 355 μm. The online temperature sensor and turbidity meter were employed to examine the experimental stages and to determine the seeding temperature, respectively.
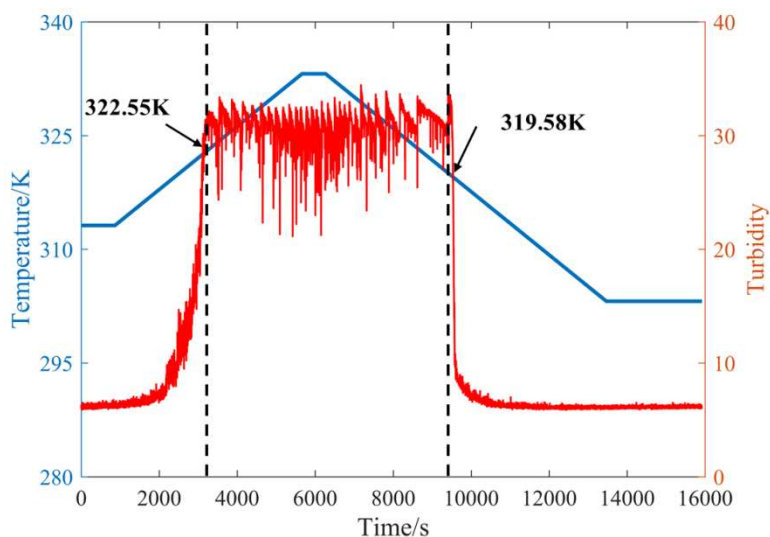
Figure 11. Determination of the seeding temperature. The blue solid line represents the temperature profile, and the red solid line shows the turbidity profile.

Figure 11 illustrates the temperature and turbidity profiles. The turbidity meter signal fell when the solution became cloudy, and the signal increased when the solution became clear. AIBN (300 g) was added into 900 g of methanol at 313.15 K, and the agitation speed was maintained at 400 rpm. After 860 s at 313.15 K, the slurry was heated at 0.25 K/min from 313.15 K to 333.15 K. During this stage, the turbidity signal increased as the AIBN dissolved and reached the highest value at 322.55 K. Then, the signal was constant until the end of the heating process. This indicated that the AIBN completely dissolved at 322.55 K. After 600 s at 333.15 K, the solution was cooled at 0.25 K/min from 333.15 K to 303.15 K. The turbidity suddenly dropped at 319.58 K, which indicated that the crystals began to form at this temperature. Consequently, the metastable zone for the experimental concentrations was between 319.58 K and 322.55 K, and the seed crystals should be added in this temperature range.
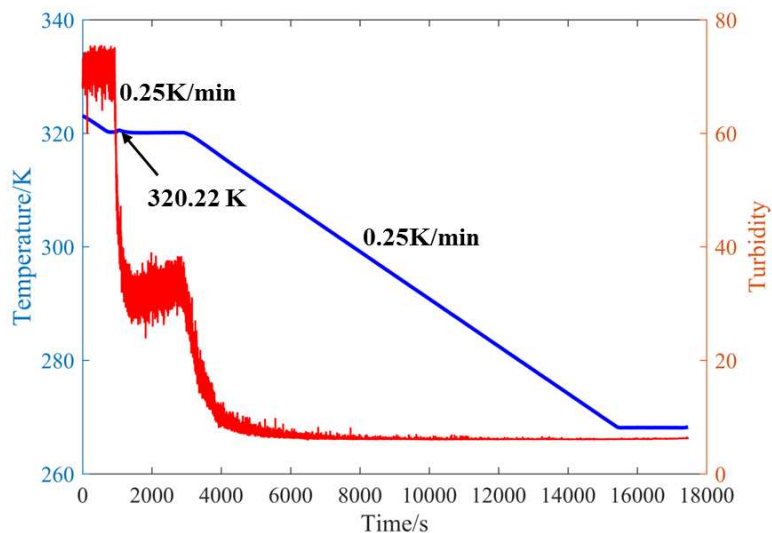
Figure 12. The experimental monitoring of the temperature and turbidity. The blue solid line represents the temperature profile, and the red solid line is the turbidity profile.

The operational conditions were optimized by sequentially adding seeds. AIBN (300 g) was dissolved in 900 g of methanol at 323.15 K, and the agitation speed was maintained at 400 rpm. The solution was then cooled at 0.25 K/min from 323.15 K to the seeding temperature (320.22 K), and 2.60 g (1% of the theoretical yield) of the crystal seeds were added to the solution as the crystal growth starting point. The slurry was maintained at that temperature for 30 min and then decreased at 0.25 K/min to 268.15 K. Figure 12 shows the monitoring plots for the temperature and turbidity. The turbidity meter was used to demonstrate the absence of primary nucleation prior to the seeding moment.

**Table 11. Comparison of the Crystallization with/without Seeding**

	operation time (minute)	yield	bulk density (g/cm^3)
unseeded	450	88%	0.72
sphere-like seeds	283	91.87%	0.68
rod-like seeds	283	90.61%	0.71
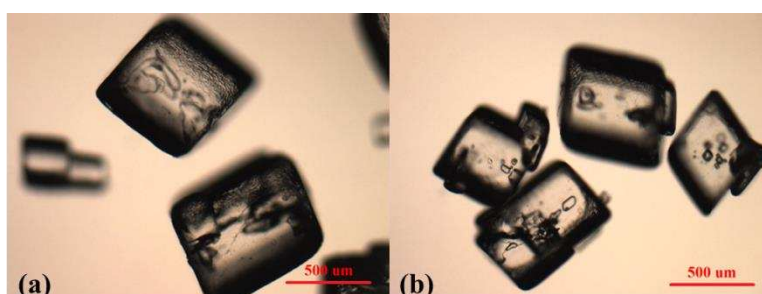
Figure 13. Morphology of the products obtained in the crystallization experiments that used seeds with different shapes: (a) sphere-like seeds and (b) rod-like seeds.

Figure 13 presents the morphologies of the products obtained from the crystallization experiments that used seeds with different shapes. The products generated from the addition of sphere-like and rod-like seeds had cubic-like shapes. The yield and bulk density were also very close, as shown in Table 11, which indicated that instead of the shape of the added seeds, the process conditions, such as the cooling rate and agitation speed, have more important roles in the yield and final product morphology of the AIBN crystals. Table 11 also shows that despite the similar bulk densities, the seeded crystallization had a higher yield in a shorter operational time than the no seed experiments.

The seeded crystallization conditions were repeated in the 20 L crystallizer but with a reduced stirring speed based on the shear force calculation. The bulk density of the prepared pilot-scale product was 0.65 g/cm^3, which was very close to that of the lab-scale product. Additionally, the product still showed good flowability after 3 months of storage in a valve bag under a kilogram weight, whereas the product before optimization showed severe caking under the same storage conditions (Figure 14). Therefore, the seeded crystallization is recommended for industrial implementation.
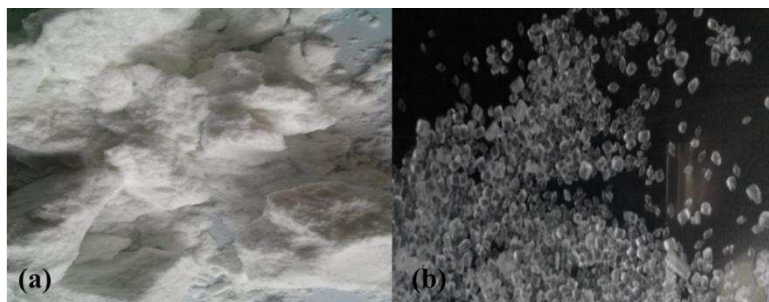
Figure 14. The product before (a) and after (b) the morphology optimization (after storage for three months).

5   Conclusion

The AIBN solubility was sensitive to the temperature in pure solvents, and the solubility values at the same temperature decreased in the following order: $x_{A,acetone} > x_{A,ethyl\,acetate} > x_{A,benzene} > x_{A,methanol} > x_{A,ethanol}$. The AIBN solubility in a mixture of methanol and water increased as the temperature and fraction of methanol increased. The calculated solubility using the modified Apelblat model showed the best fit for the experimental data for the pure solvents and a mixture of methanol and water. Two polymorphic forms of the AIBN crystals based on form I in a monoclinic cell and form II in a triclinic cell were prepared via crystallization. The initial concentration and cooling rate are the main factors that determine the

polymorphic forms of the AIBN crystals. The crystallization process was optimized using unseeded and seeded crystallization processes to yield polymorphic I AIBN crystals with an ideal morphology that preventing crystal caking. The seeded crystallization condition induced a higher yield and shorter production time and is recommended for industry implementation after it was tested in a 20 L pilot-scale crystallizer.
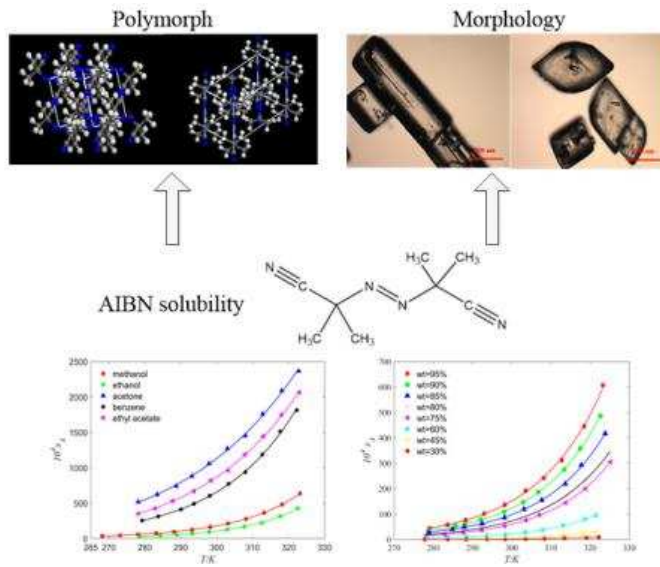
Supporting Information. Comparison of experimental solubility of AIBN in methanol and data from literature.[13]

References

(1) Li, X. R.; Wang, X. L.; Koseki, H. Study on thermal decomposition characteristics of AIBN. J. Hazard. Mater. **2008,** 159, 13-18.

(2) Roduit, B.; Hartmann, M.; Folly, P.; Sarbach, A.; Brodard, P.; Baltensperger, R. Thermal decomposition of AIBN, Part B: Simulation of SADT value based on DSC results and large scale tests according to conventional and new kinetic merging approach. Thermochim. Acta **2015,** 621, 6-24.

(3) Peng, M. J.; Lu, G. B.; Chen, W. H.; Chen, L. P.; Lü, J. Y. Thermal Decomposition Characteristic and Kinetics of AIBN in Aniline Solvent. Acta Phys. Chim. Sin. **1993,** 29, 2095-2100(6).

(4) Jaffe, A. B.; Skinner, K. J.; Mcbride, J. M. Solvent steric effects. II. Free-radical chemistry of azobisisobutyronitrile and azobis-3-cyano-3-pentane in viscous and crystalline media. J. Am. Chem. Soc. **2002,** 94, 721-727.

(5) Zhang, R.; Feng, Z.; Ji, H. Measurement and Correlation of Solubility of Two Isomers of Cyanopyridine in Eight Pure Solvents from 268.15 K to 318.15 K. J. Chem. Eng. Data **2017,** 62, 3241-3251.

(6) Apelblat, A.; Manzurola, E. Solubilities of o -acetylsalicylic, 4-aminosalicylic, 3,5-dinitrosalicylic, and p -toluic acid, and magnesium- DL -aspartate in water from T =(278 to 348) K. J. Chem. Thermodyn. **1999,** 31, 85-91.

(7) Hao, H.; Wang, J.; Wang, Y. Solubility of Dexamethasone Sodium Phosphate in Different Solvents. J. Chem. Eng. Data **2004,** 49, 1697-1698.

(8) Liu, Y.; Wang, J.; Wang, X.; Liu, P.; Pang, F. Solubility of Valsartan in Different Organic Solvents and

Ethanol + Water Binary Mixtures from (278.15 to 313.15) K. J. Chem. Eng. Data **2009,** 54, 986-988.

(9) Wilson, G. M. Vapor-Liquid Equilibrium. XI. A New Expression for the Excess Free Energy of Mixing. J. Am. Chem. Soc. **1964,** 86, 127-130.

(10) Zhang, Y.; Liu, J. J.; Zhang, L.; Wang, X. Z. Solubility of 2,5-Di-tert-butylhydroquinone and Process Design for Its Purification Using Crystallization. J. Chem. Eng. Data **2015,** 60, 1968-1974.

(11) Buchowski, H.; Ksiazczak, A.; Pietrzyk, S. Solvent activity along a saturation line and solubility of hydrogen-bonding solids. J. Phys. Chem. **1980,** 84, 975-979.

(12) Dun, W.; Wu, S.; Tang, W.; Wang, X.; Sun, D.; Du, S.; Gong, J. Solubility of Ibuprofen Sodium Dihydrate in Acetone + Water Mixtures: Experimental Measurement and Thermodynamic Modeling. J. Chem. Eng. Data **2014,** 59, 3415-3421.

(13) Zhou, S. S.; Liang, J. Z.; Chen, X. P.; Wang, L. L.; Wei, X. J.; Pang, D. F.; Zhou, D. Q. Determination and correlation of the solubility for azobisisobutyronitrile in methanol and dimethyl carbonate. J.Guangxi Univ.(Nat Sci Ed) **2016,** 41, 1629-1635.

(14) Smallwood, I. M. Handbook of Organic Solvent Properties. Wiley: New York, 1996.

(15) Jaffe, A. B.; Malament, D. S.; Slisz, E. P.; Mcbride, J. M. Solvent steric effects. III. Molecular and crystal structures of azobisisobutyronitrile and azobis-3-cyano-3-pentane. Structural deuterium isotope effect. J. Am. Chem. Soc. **1972,** 94, 8515-8521.

(16) Roduit, B.; Hartmann, M.; Folly, P.; Sarbach, A.; Brodard, P.; Baltensperger, R. Determination of thermal hazard from DSC measurements. Investigation of self-accelerating decomposition temperature (SADT) of AIBN. J. Therm. Anal. Calorim. **2014,** 117, 1017-1026.

(17) Cardew, P. T.; Davey, R. J. The Kinetics of Solvent-Mediated Phase Transformations. Proc. R. Soc. London, Ser. A **1985,** 398, 415-428.

(18) Mangin, D.; Puel, F.; Veesler, S. Polymorphism in Processes of Crystallization in Solution: A Practical Review. Org. Process Res. Dev. **2009,** 13, 1241-1253.

(19) Cheng, H. J.; Hsiau, S. S. The study of granular agglomeration mechanism. Powder Technol. **2010,** 199, 272-283.

(20) Scholl, S. K.; Schmidt, S. J. Determining the physical stability and water–solid interactions responsible for caking during storage of glucose monohydrate. J.Food Meas.Charact. **2014,** 8, 316-325.

(21) Chen, M.; Lin, L.; Zhang, Y.; Wu, S.; Liu, E.; Wang, K.; Wang, J. Mechanism and inhibition of trisodium phosphate particle caking: Effect of particle shape and solubility. Particuology **2016,** 27, 115-121.

Polymorph

Morphology

AIBN solubility

For Table of Contents Only